

An Adaptive Environment-Aware Transformer Autoencoder for UAV-FSO with Dynamic Complexity Control

Han Zeng*, Haibo Wang*, *Member, IEEE*, Kan Wang, Xutao Yu, Zaichen Zhang, *Senior Member, IEEE*

Abstract—The rise of sixth-generation (6G) wireless networks sets high demands on UAV-assisted Free Space Optical (FSO) communications, where the channel environment becomes more complex and variable due to both atmospheric turbulence and UAV-induced vibrations. These factors increase the challenge of maintaining reliable communication and require adaptive processing methods. Autoencoders are promising as they learn optimal encodings from channel data. However, existing autoencoder designs are generic and lack the specific adaptability and computational flexibility needed for UAV-FSO scenarios. To address this, we propose AEAT-AE (Adaptive Environment-aware Transformer Autoencoder), a Transformer-based framework that integrates environmental parameters into both encoder and decoder via a cross-attention mechanism. Moreover, AEAT-AE incorporates a Deep Q-Network (DQN) that dynamically selects which layers of the Transformer autoencoder to activate based on real-time environmental inputs, effectively balancing performance and computational cost. Simulation results demonstrate that AEAT-AE outperforms conventional methods in bit error rate while maintaining efficient runtime, representing a novel tailored solution for next-generation UAV-FSO communications.

Index Terms—Autoencoder, Transformer, optical wireless communication, DQN, UAV-FSO

I. INTRODUCTION

AS the development of sixth-generation (6G) wireless networks advances, requirements for ultra-high data rates, massive connectivity, and low latency continue to intensify. These demands, driven by applications such as high-definition video streaming, distributed edge computing, and industrial Internet of Things (IoT) systems, further exacerbate the limitations of the already crowded radio frequency (RF) spectrum [1]. In this context, Free Space Optical (FSO) communication, a key technology within Optical Wireless Communication

(OWC), has emerged as a promising solution to support future high-capacity wireless links due to its inherent advantages, including extremely high bandwidth, immunity to RF interference, low latency, and enhanced security [2]–[4].

The integration of Unmanned Aerial Vehicles (UAVs) with FSO communication has become a key enabler for 6G networks, addressing critical needs for flexible coverage extension and rapid deployment in disaster recovery operations where ground infrastructure is compromised, remote area communications lacking fiber backhaul, and dense urban environments requiring high-capacity links [5]–[7]. UAV-mounted FSO terminals provide reconfigurable line-of-sight connectivity for backhaul, relaying, and direct access services [8]–[12].

However, this integration introduces two compounded channel impairments: (1) persistent beam misalignment caused by UAV platform jitter and mobility [13], and (2) signal degradation due to atmospheric turbulence and weather effects [14]. Extensive research has established and utilized mathematical models for UAV-FSO channel characterization, which serve as the foundation for system modeling and simulation in many works. Using these models for end-to-end system performance analysis, however, often requires significant simplifications due to the complexity and dynamic nature of the environment. This challenge motivates the adoption of data-driven machine learning techniques, which can leverage simulated data based on these models to discover underlying patterns and enable adaptive optimization beyond the reach of purely analytical approaches.

As shown in Fig. 1 (a), prior research has focused on improving individual components of the communication pipeline. Machine learning methods like support vector machines (SVMs) and deep learning have enhanced detector adaptation for better decoding under varying channels [15]–[17]. Convolutional neural networks (CNNs) have been used to predict channel fluctuations, enabling proactive system adjustments [18], [19]. However, these methods typically optimize components separately, limiting end-to-end performance in dynamic airborne environments. Without joint optimization, the system struggles to maintain stable communication amid UAV mobility and atmospheric disturbances.

To address these limitations, recent efforts have focused on learning-based methods that enable end-to-end optimization. In particular, autoencoder (AE)-based models have gained traction for their ability to model the entire communication system—encoder, channel, and decoder—within a unified, differentiable framework, as shown in Fig. 1 (b).

*Han Zeng and Haibo Wang contributed equally to this work.

This work is supported by NSFC projects (62471126, 623B2017 and 61960206005), the Fundamental Research Funds for the Central Universities 2242022k60001, Jiangsu Key R&D Program Project BE2023011-2, the research fund of National Mobile Communications Research Lab. 2025A03. (Corresponding author: Zaichen Zhang.)

Han Zeng, Haibo Wang and Zaichen Zhang are with the National Mobile Communications Research Laboratory, Southeast University, Nanjing 210096, P.R.China, and they are also with the Purple Mountain Laboratory, Nanjing 211111, P. R. China. (e-mail: 230228224@seu.edu.cn, haibowang@seu.edu.cn, zczhang@seu.edu.cn)

Kan Wang is with the Purple Mountain Laboratory, Nanjing 211111, P. R. China. (e-mail: wangkan@pmlabs.com.cn)

Xutao Yu is with the State Key Lab of Millimeter Waves, Southeast University, Nanjing 210096, P. R. China, and also with the Purple Mountain Laboratory, Nanjing 211111, P. R. China. (e-mail: yuxutao@seu.edu.cn)

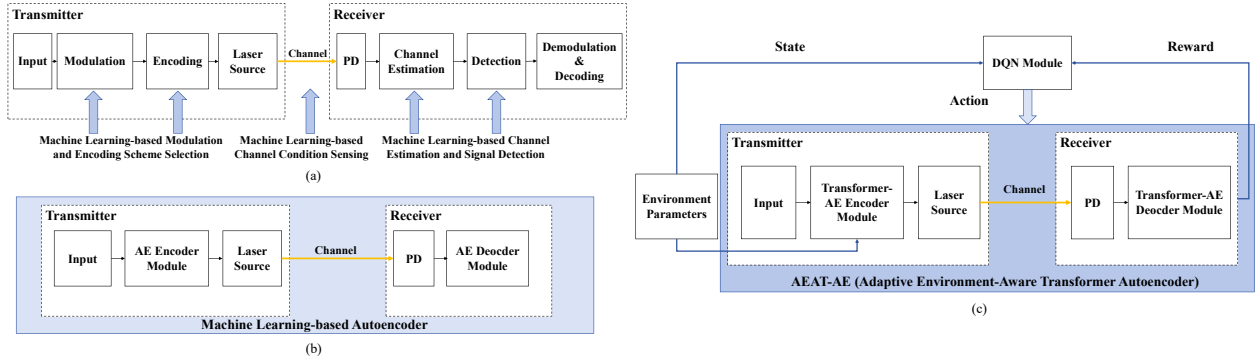


Fig. 1. Comparison of schemes for applying machine learning to the transmission process of communication systems: (a) machine learning optimization for specific modules; (b) The system model of traditional end-to-end autoencoder; (c) The system model proposed in this work.

TABLE I
RELATED WORKS

| Ref. | RF or Optical | Main Propose | Main Contribution | Main Network or Model | Main Comparative Indicators |
|-------------|---------------|-------------------------|---|-----------------------|-----------------------------|
| [20] (2017) | RF | End-to-End Optimization | Introduces the use of AE for end-to-end communication systems | DNN (FCN) | BLER |
| [21] (2018) | RF | Model-Free Channel AE | Optimizes AE without channel gradients | DNN (FCN) | BER |
| [22] (2018) | Optical (OWC) | End-to-End Optimization | Introduces autoencoder-based optical wireless communication systems | DNN (FCN) | BLER |
| [23] (2019) | RF | Model-Free Channel AE | Introduces a RL-based AE without gradient backpropagation | RL | BLER, PSNR |
| [24] (2019) | Optical (OWC) | End-to-End Optimization | Introduces autoencoder-based transceivers | DNN (FCN) | BLER |
| [25] (2020) | RF | Model-Free Channel AE | Introduces an end-to-end communication system using conditional GANs to model wireless channels | CNN & GAN | BLER & BER |
| [26] (2020) | RF | JSCC with Feedback | Introduces CNN-based AE using multiple encoder-decoder pairs for progressive transmission | CNN | PSNR |
| [27] (2020) | Optical (OWC) | End-to-End Optimization | Introduces AE based asymmetrically-clipped optical OFDM communication system | ReLU+IFFT/FFT | BER |
| [28] (2022) | Optical (FSO) | End-to-End Optimization | Introduces AE-based free space optical communication systems | DNN (FCN) | BER |
| [29] (2023) | Optical (FSO) | End-to-End Optimization | Introduces learning-based autoencoder for multiple access and interference channels | DNN (FCN) | BER |
| [30] (2024) | Optical (FSO) | End-to-End Optimization | Introduces an end-to-end AE in non-differentiable Poisson channel | DNN (FCN) | BER |
| [31] (2024) | Optical (OWC) | End-to-End Optimization | Introduces a differential AE for OWC systems | DNN (FCN) | BER |

A. Prior Works

Existing AE-based communication systems have evolved along three main research directions, as summarized in Table I. Early works (2017–2019) proposed basic AE architectures using fully connected networks (FCNs) in both RF [20], [21] and optical [22], [24] domains, focusing on metrics such as bit error rate (BER) and block error rate (BLER). Later developments (2019–2020) explored new training paradigms—including reinforcement learning [23] and GAN-based channel modeling [25]—alongside architectural advances like CNN-based joint source-channel coding (JSCC) [26] and optical OFDM [27]. More recent efforts (2020–2024) have targeted FSO-specific challenges, including Poisson channel non-differentiability [30], multi-user interference [29], turbulence resilience [28], and differential coding [31].

Most of these approaches are built upon widely adopted

channel models and rely on simulated datasets, which facilitate reproducibility and controllable experimentation. While this simulation-based approach remains standard and is also adopted in our work, existing methods still face three major limitations when applied to UAV-FSO systems: (1) most are not specifically designed for UAV-FSO scenarios, focusing instead on generic FSO or RF environments; (2) their black-box architectures lack adaptability to environmental variation; and (3) channel parameters are only loosely incorporated, often treated as optional inputs rather than integral parts of the encoding process. These limitations become particularly critical in UAV-FSO links, where atmospheric turbulence and misalignment-induced fading create highly dynamic and non-linear channel conditions, making robust adaptation essential.

B. Our Contributions

To address these limitations in UAV-FSO settings, we propose the **Adaptive Environment-Aware Transformer**

Autoencoder (AEAT-AE), a Transformer-based framework tailored for UAV-FSO systems. As shown in Fig. 1 (c), AEAT-AE performs end-to-end optimization by jointly modeling transmitter and receiver, while embedding environmental parameters directly into both encoding and decoding. The Transformer's symmetric encoder-decoder structure aligns naturally with the AE paradigm: the encoder learns compact latent representations, and the decoder reconstructs the signal under channel distortions. Multi-head attention captures diverse channel characteristics, enabling robust adaptation under highly dynamic conditions.

Given the high computational cost associated with Transformers, we further enhance AEAT-AE's adaptability by integrating a **Deep Q-Network (DQN)-based dynamic layer selection mechanism**. The DQN controller learns to activate only the most relevant Transformer layers during inference, enabling the model to adjust its computational load based on real-time environmental conditions. Unlike heuristic or rule-based approaches, which struggle with the complexity and variability of UAV-FSO channels, the DQN offers a more scalable and data-driven solution. This mechanism operates at the inference stage, dynamically adjusting the computation graph to balance performance and efficiency in response to channel dynamics.

We summarize the main contributions of this work as follows:

(1) Environment-Integrated Transformer AE Design: We propose a novel Transformer-based autoencoder architecture, AEAT-AE, that seamlessly incorporates environmental parameters into both the encoding and decoding processes. This approach improves the model's adaptability to diverse UAV-FSO channel conditions, overcoming the limitations of traditional AE models that treat environmental information as isolated inputs.

(2) Dynamic Inference Optimization via DQN: AEAT-AE incorporates a DQN-based dynamic layer selection strategy that adaptively adjusts the inference path based on environmental conditions and system constraints. This enables efficient control over model complexity without retraining, significantly reducing computation under stable conditions while enhancing adaptability in dynamic environments.

(3) Improved Performance and Efficiency: Extensive simulation results, including ablation studies, demonstrate that AEAT-AE achieves comparable or superior BER performance compared to traditional autoencoder schemes such as CNN- and FCN-based models. Leveraging the DQN-based dynamic layer selection, AEAT-AE significantly reduces computational complexity and enhances system efficiency under varying UAV-FSO conditions, all without compromising accuracy.

C. Organization

The rest of the paper is organized as follows: Section II introduces the system and channel models for UAV-FSO systems. Section III presents the proposed AEAT-AE framework, detailing the Transformer-based encoder-decoder architecture and the DQN-based dynamic layer selection mechanism. Section IV provides experimental results and performance

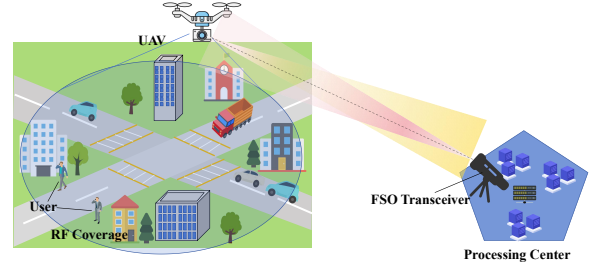


Fig. 2. One application scenario of UAV-FSO systems.

evaluation. Section V discusses the results and future work, and Section VI concludes the paper.

II. SYSTEM MODEL

A. AE-Based UAV-FSO System Model

Fig. 2 shows a typical UAV-FSO scenario, where a data center established a high-capacity optical link to a UAV providing RF coverage over a target area. The UAV-FSO link quality is highly sensitive to UAV jitter and atmospheric turbulence, resulting in time-varying and challenging channel conditions. To ensure robust and adaptive communication, we adopt an AE-based system that jointly learns transmitter and receiver mappings in an end-to-end manner, enabling data-driven adaptation to complex channel dynamics. The AE encoder compresses the input bitstream $\mathbf{s} \in \{0, 1\}^N$ into a vector $\mathbf{x} \in \mathbb{R}^K$ for transmission over the UAV-FSO link.

We employ On-Off Keying (OOK) modulation due to its simplicity, low power consumption, and compatibility with intensity modulation/direct detection (IM/DD) schemes, making it suitable for UAV optical transceivers with strict size, weight, and power constraints. The received signal at the receiver, denoted by \mathbf{y} , is given by:

$$\mathbf{y} = \eta_e P_t \mathbf{H} \mathbf{x} + \mathbf{w}, \quad (1)$$

where η_e is the photodetector's responsivity, \mathbf{x} is the transmitted symbol vector, \mathbf{H} is the channel coefficient matrix, P_t is the transmit power, and $\mathbf{w} \sim N(0, \sigma_w^2 \mathbf{I}_n)$ denotes the Gaussian noise vector, σ_w^2 is the noise variance.

At the receiver, the AE decoder reconstructs the signal $\hat{\mathbf{s}} \in \{0, 1\}^N$. The goal is to adjust the AE's internal parameters to minimize the binary cross entropy between \mathbf{s} and $\hat{\mathbf{s}}$:

$$\min \sum_{n=1}^N (s_n \log(\hat{s}_n) + (1 - s_n) \log(1 - \hat{s}_n)). \quad (2)$$

B. Channel Fading Model for UAV-FSO Systems

The UAV-FSO channel presents distinct challenges compared to traditional OWC systems, primarily due to its heightened sensitivity to beam misalignment, UAV-induced motion, and atmospheric turbulence. These dynamic factors induce substantial fluctuations in the channel coefficient \mathbf{H} , necessitating a modeling approach that balances realism and analytical tractability.

In this work, we employ a widely recognized channel fading model that encapsulates both internal disturbances (e.g.,

platform vibration, mechanical jitter) and external factors (e.g., wind, turbulence) into a unified stochastic jitter parameter. **This modeling strategy, which has been extensively validated in the UAV-FSO literature [4]–[6], [8], [14], [35]–[37], facilitates controlled and repeatable evaluation of system performance.** Such consistency is often difficult to achieve in hardware results due to the presence of noise, measurement errors, and unmodeled physical effects.

We focus on evaluating the adaptability of the Transformer-AE framework under dynamic conditions using a simulation-based approach for its analytical clarity. Instead of proposing a brand new channel model, we leverage an established abstraction to investigate Transformer-based adaptation in UAV-FSO systems. To capture the composite effects involved, the overall channel coefficient is modeled as:

$$h = h_l h_a h_p h_{AoA}, \quad (3)$$

where h_l is the atmospheric attenuation resulting from the scattering and absorption phenomena, modeled by the Beer-Lambert law: $h_l = \exp(-Z\xi)$, with Z as the link distance and ξ as the scattering coefficient influenced by visibility distance V_d . h_a is the atmospheric turbulence fading, h_p is the pointing error fading and h_{AoA} denotes the link interruption due to radial angle of arrival (AoA) fluctuations.

1) *Atmospheric Turbulence h_a* : This fading is caused by temperature and density fluctuations. We choose the Málaga distribution to cover both weak and strong turbulence conditions [35]. The distribution of h_a is:

$$f_{h_a}(h_a) = A \sum_{k=1}^{\beta} \left(a_k h_a^{\frac{\alpha+k}{k}-1} \right) K_{\alpha-k} \left(2\sqrt{\frac{\alpha\beta h_a}{b\beta + \Omega'}} \right), \quad (4)$$

$$\begin{cases} A = \frac{2\alpha^{\frac{\alpha}{2}}}{b^{1+\frac{\alpha}{2}} \Gamma(\alpha)} \left(\frac{b\beta}{b\beta + \Omega'} \right)^{\beta + \frac{\alpha}{2}}, \\ a_k = \left(\frac{\beta-1}{k-1} \right) \frac{(b\beta + \Omega')^{1-\frac{k}{2}}}{(k-1)!} \left(\frac{\Omega'}{b} \right)^{k-1} \left(\frac{\alpha}{\beta} \right)^{\frac{k}{2}}, \end{cases} \quad (5)$$

$$\Omega' = \Omega + \rho 2b_0 + 2\sqrt{2b_0\Omega\rho} \cos(\phi_A - \phi_B), \quad (6)$$

$$\rho = (0.55C_n^2\lambda^2)^{-3/5}, \quad (7)$$

where α is the number of large-scale cells, β is the fading parameter, $\sigma_R^2 = 1.23C_n^2k^{7/6}Z^{11/6}$ is the Rytov variance, K_v is the modified Bessel function of second kind of order v , $\phi_A - \phi_B$ is the phase difference, ρ is the coherence length, $b = 2b_0(1 - \rho)$ is the average scattering power, $2b_0$ is the total scatter power, λ is the beam wavelength, C_n^2 is the refractive index structure, Ω is the LoS power, and Ω' is the coherent power.

2) *Point Error due to Transmitter and UAV Jitter h_p* : UAV mobility and mechanical vibrations of platforms cause pointing errors, leading to misalignment between the transmitter and receiver. For a Gaussian beam at the receiver, power loss due to radial displacement r_d is:

$$h_p \approx A_0 \exp\left(-\frac{2r_d^2}{w_z^2}\right), \quad (8)$$

where A_0 is the power fraction at zero pointing error and can be presented as:

$$A_0 = \text{erf}(v)^2, v = \sqrt{\frac{\pi}{2}} \frac{r_a}{w_z}, \quad (9)$$

$$w_z \approx w_{oz} \sqrt{1 + \Theta \left(\frac{\lambda Z}{\pi w_{oz}^2} \right)^2}, \Theta = 1 + \frac{2w_{oz}^2}{\rho^2}, \quad (10)$$

where $\text{erf}(\cdot)$ represents the error function, w_z is the Gaussian beamwaist, w_{oz} is the beamwidth at $Z = 0$, r_a is the receiver lens radius, and C_n^2 is the refractive index structure parameter.

UAV jitter, caused by factors like hardware structure, payload, and gimbal control, increases radial displacement from the beam center to the receiving aperture. This jitter is often modeled as a Gaussian-distributed random variable, and the total radial displacement $r_d = \sqrt{x_d^2 + y_d^2}$ follows a Beckmann distribution [35]–[37]. Since its PDF lacks a closed-form expression, a modified Rayleigh distribution is used for approximation:

$$f_{h_p}(h_p) = \frac{g^2}{A_0^{g^2}} h_p^{g^2-1}, \quad (11)$$

where $g = \frac{w_{zeq}}{2\sigma_s}$, $w_{zeq} = \frac{w_z^2 \sqrt{2} \text{erf}(v)}{2v \exp(-v^2)}$ is the equivalent beam radius, and σ_s is the pointing error standard deviation.

3) *Fading due to AoA Fluctuations caused by UAV Motion h_{AoA}* : In UAV-to-Ground (U2G) FSO scenarios, the deviation in angle of arrival (AoA) is defined as $\theta_{AoA} = \sqrt{\theta_{tx}^2 + \theta_{ty}^2}$, where θ_{tx} and θ_{ty} denote the boresight bias angles caused by UAV jitter, turbulence, and platform disturbances. A commonly adopted model in UAV-FSO studies [35]–[37] assumes that if the AoA exceeds the receiver's field of view (FoV), the signal is lost and $h_{AoA} = 0$; otherwise, $h_{AoA} = 1$:

$$h_{AoA} = \begin{cases} 1, & \theta_{AoA} \leq \theta_{FoV} \\ 0, & \theta_{AoA} > \theta_{FoV} \end{cases} \quad (12)$$

To model its stochastic behavior, we adopt a Beckmann-based distribution:

$$f_{h_{AoA}}(h_{AoA}) = S\delta(h_{AoA}) + (1 - S)\delta(h_{AoA} - 1), \quad (13)$$

where $S = \exp\left(-\frac{\theta_{FoV}^2}{2\sigma_a^2}\right)$, with σ_a representing the standard deviation of angular jitter.

To explicitly characterize the stochastic nature of AoA fluctuations, the distribution of θ_{AoA} is approximated as:

$$f_{\theta_a}(\theta_a) \approx \frac{\theta_a}{\sigma_a^2} \exp\left(-\frac{\theta_a^2}{2\sigma_a^2}\right), \quad \theta_a \geq 0, \quad (14)$$

where σ_a^2 encapsulates the UAV's orientation instability. For U2G links, it is given by:

$$\sigma_a^2 = \left(\frac{3\theta_{tx}^2\sigma_{txo}^4 + 3\theta_{ty}^2\sigma_{tyo}^4 + \sigma_{txo}^6 + \sigma_{tyo}^6}{2} \right)^{\frac{1}{3}}, \quad (15)$$

where σ_{txo} and σ_{tyo} denote the standard deviations of the transmitter UAV's orientation in the x - z and y - z planes, respectively, θ'_{tx} and θ'_{ty} denote the UAV boresight angle.

Despite its simplicity, this model directly reflects UAV-induced effects such as jitter, wind deviations, and flight instability, which lead to misalignment and signal blockage. It is widely used in UAV-FSO research for its balance between interpretability and analytical tractability.

III. ADAPTIVE ENVIRONMENT-AWARE TRANSFORMER AUTOENCODER (AEAT-AE) FRAMEWORK

In this section, we propose the AEAT-AE framework and detail how environmental awareness, Transformer encoding, and DQN-based adaptation are integrated into a unified architecture for dynamic and intelligent resource allocation.

A. Latent Representation Design for Joint Signal and Environment Awareness

Before entering the Transformer layers, both the input signal and the environmental parameters must be embedded into a unified latent space to ensure compatibility and facilitate joint processing.

1) *Tokenizing and Embedding Binary Signals for AEAT-AE Encoding:* The original binary input $\mathbf{s} \in \{0, 1\}^N$ is first reshaped into a sequence of tokens, forming $\mathbf{X}_0 \in \mathbb{R}^{T \times d_{in}}$, where T is the sequence length and d_{in} is the input feature dimension per token. It is then linearly projected to match the Transformer's input dimension:

$$\mathbf{X} = \mathbf{X}_0 \mathbf{W}_{sig} + b_{sig}, \quad \mathbf{W}_{sig} \in \mathbb{R}^{d_{in} \times d_k}, b_{sig} \in \mathbb{R}^{d_k} \quad (16)$$

where \mathbf{W}_{sig} and b_{sig} are the trainable projection matrix and bias vector, respectively, and d_k denotes the embedding dimension used within the Transformer layers.

2) *Processing and Embedding Environmental States for AEAT-AE Adaptation:* The proposed environment representation $\mathbf{E} = [Z, V_d, C_n^2, \sigma_s, \sigma_a]$ includes five parameters: link distance Z , visibility V_d , refractive index structure parameter C_n^2 , pointing error σ_s , and UAV jitter σ_a . While these parameters are not always directly available on standard UAV platforms, they can be estimated using lightweight, practical methods. For example, Z and V_d can be obtained from GPS or flight planning data; C_n^2 can be estimated using standard turbulence models based on altitude, temperature, or received signal characteristics; and σ_s and σ_a can be inferred from IMU or gyroscope readings. These sensors are either standard or easily integrable in modern UAV systems. Although some estimates may involve approximation or latency, our design does not rely on high-precision, real-time measurements. The goal is to extract coarse environmental trends to guide Transformer adaptation, not to build an exact sensing system.

To align these heterogeneous features with the Transformer's input space, \mathbf{E} is projected via a multi-layer perceptron (MLP):

$$\mathbf{E}_{in} = \sigma_E(\mathbf{E} \mathbf{W}_{env} + b_{env}), \quad \mathbf{W}_{env} \in \mathbb{R}^{5 \times d_k}, b_{env} \in \mathbb{R}^{d_k}, \quad (17)$$

where $\sigma_E(\cdot)$ is the nonlinear activation function, and \mathbf{W}_{env} , b_{env} are learnable parameters of the MLP. This transformation allows the environment information to be effectively integrated into the model through cross-attention mechanisms.

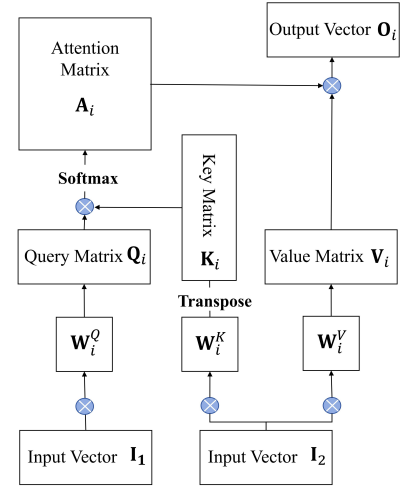


Fig. 3. Illustration of the Attention Mechanism in Transformer Models.

B. Attention Mechanisms and Environment Fusion in AEAT-AE

Our proposed AEAT-AE employs Transformer's dual attention: self-attention for signal dependencies and cross-attention for environmental fusion, enabling dynamic feature adaptation to UAV-FSO channel variations.

As shown in Fig. 3, the Transformer encoder consists of stacked layers with self-attention and cross-attention. The first layer takes input $\mathbf{X} \in \mathbb{R}^{T \times d}$, where T is sequence length and d is feature dimension. Subsequent layers use $\mathbf{I}^{(l)}$, the output from the previous layer, refining the representation.

1) *Signal Feature Extraction via Multi-Head Self-Attention:* At the l -th layer, multi-head self-attention processes $\mathbf{I}^{(l)} \in \mathbb{R}^{T \times d}$, capturing dependencies within the sequence. With N_h heads, the model attends to multiple representation subspaces simultaneously. For each head, queries, keys, and values are computed as:

$$\begin{aligned} \mathbf{Q}_i^{(l)} &= \mathbf{I}^{(l)} \mathbf{W}_i^{Q,(l)}, \\ \mathbf{K}_i^{(l)} &= \mathbf{I}^{(l)} \mathbf{W}_i^{K,(l)}, \\ \mathbf{V}_i^{(l)} &= \mathbf{I}^{(l)} \mathbf{W}_i^{V,(l)}, \end{aligned} \quad (18)$$

where $\mathbf{W}_i^{Q,(l)}, \mathbf{W}_i^{K,(l)} \in \mathbb{R}^{d \times d_k}$ and $\mathbf{W}_i^{V,(l)} \in \mathbb{R}^{d \times d_v}$ are learnable parameters. The attention weights are computed using scaled dot-product attention:

$$\mathbf{A}_i^{(l)} = \text{Softmax} \left(\frac{\mathbf{Q}_i^{(l)} (\mathbf{K}_i^{(l)})^\top}{\sqrt{d_k}} \right), \quad (19)$$

where the softmax function normalized the scores for numerical stability. It is followed by the head-wise output:

$$\mathbf{O}_i^{(l)} = \mathbf{A}_i^{(l)} \mathbf{V}_i^{(l)}. \quad (20)$$

The outputs from all heads are concatenated and linearly transformed to produce the self-attention output:

$$\mathbf{O}_{self}^{(l)} = \text{Concat}(\mathbf{O}_1^{(l)}, \dots, \mathbf{O}_{N_h}^{(l)}) \mathbf{W}^{O,(l)}, \quad (21)$$

where $\mathbf{W}^{O,(l)} \in \mathbb{R}^{N_h d_v \times d}$ is the output projection matrix.

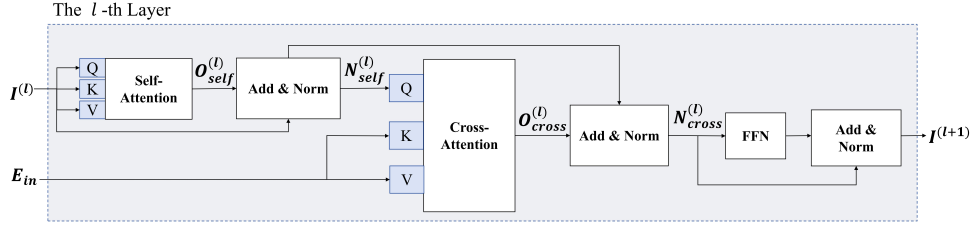


Fig. 4. Unified Transformer Layer.

2) *Environmental Feature Fusion via Cross-Attention:* To incorporate environmental information, each layer includes a cross-attention module. The self-attention output $\mathbf{O}_{\text{self}}^{(l)}$ is first combined with the layer input $\mathbf{I}^{(l)}$ via a residual connection, followed by layer normalization to produce $\mathbf{N}_{\text{self}}^{(l)}$, which serves as the query in the cross-attention. The environmental sequence $\mathbf{E}_{\text{in}} \in \mathbb{R}^{T_e \times d}$, shared across all layers, is used as both the key and value.

The attention mechanism in this cross-attention module is similar to that in self-attention, where the query $\mathbf{Q}_i^{c,(l)}$, key $\mathbf{K}_i^{c,(l)}$, and value $\mathbf{V}_i^{c,(l)}$ are computed as:

$$\begin{aligned} \mathbf{Q}_i^{c,(l)} &= \mathbf{N}_{\text{self}}^{(l)} \mathbf{W}_i^{Q_c,(l)}, \\ \mathbf{K}_i^{c,(l)} &= \mathbf{E}_{\text{in}} \mathbf{W}_i^{K_c,(l)}, \\ \mathbf{V}_i^{c,(l)} &= \mathbf{E}_{\text{in}} \mathbf{W}_i^{V_c,(l)}. \end{aligned} \quad (22)$$

Here, $\mathbf{W}_i^{Q_c,(l)}, \mathbf{W}_i^{K_c,(l)} \in \mathbb{R}^{d \times d_k}$ and $\mathbf{W}_i^{V_c,(l)} \in \mathbb{R}^{d \times d_v}$ are learnable parameters within the cross attention process. The attention weights are computed through scaled dot-product attention similar to the operations in (19) and (20), with the output of $\mathbf{O}_{N_i}^{c,(l)}$. The final fused output $\mathbf{O}_{\text{cross}}^{(l)}$ is obtained by concatenating the outputs of all attention heads and applying a linear transformation:

$$\mathbf{O}_{\text{cross}}^{(l)} = \text{Concat}(\mathbf{O}_1^{c,(l)}, \dots, \mathbf{O}_{N_h}^{c,(l)}) \mathbf{W}^{O_c,(l)}.$$

This fused output $\mathbf{O}_{\text{cross}}^{(l)}$ incorporates the environmental information to adjust the self-attention output, allowing the model to jointly attend to both the signal and environmental contexts.

C. Transformer-Based Autoencoder in AEAT-AE

1) *Unified Transformer Layer for AEAT-AE:* The input embedding and attention mechanism form the foundational components of our proposed AEAT-AE, which employs a Transformer-AE as its backbone architecture. A key feature of this design is the shared Transformer layer structure between encoder and decoder (Fig. 4), where each layer integrates the following modules:

- **Self-Attention Module:** Captures intra-modal dependencies within the signal embedding.
- **Cross-Attention Module:** Integrates environmental context into the signal representation.
- **Feedforward Network (FFN) and Layer Normalization:** Enhances feature transformation and stabilizes training.

a) *Self-Attention Module:* The self-attention mechanism refines the signal representation by capturing intra-modal relationships. The output of multi-head self-attention is:

$$\mathbf{O}_{\text{self}}^{(l)} = \text{SelfAttention}(\mathbf{I}^{(l)}), \quad (23)$$

where $\mathbf{O}_{\text{self}}^{(l)} \in \mathbb{R}^{T \times d}$ is the self-attended signal feature.

b) *Cross-Attention Module:* To fuse external environmental information, we apply cross-attention between the self-attended output $\mathbf{O}_{\text{self}}^{(l)}$ and the embedded environmental sequence \mathbf{E}_{in} :

$$\mathbf{O}_{\text{cross}}^{(l)} = \text{CrossAttention}(\mathbf{O}_{\text{self}}^{(l)}, \mathbf{E}_{\text{in}}), \quad (24)$$

where $\mathbf{O}_{\text{cross}}^{(l)} \in \mathbb{R}^{T \times d}$ produces environment-conditioned features for downstream processing.

c) *Feed-Forward Network and Layer Normalization:* The output of each attention module undergoes a series of standard Transformer operations: residual connection, layer normalization, and position-wise FFN.

First, the self-attention output $\mathbf{O}_{\text{self}}^{(l)}$ is combined with the layer input $\mathbf{I}^{(l)}$ through residual connection and layer normalization:

$$\mathbf{N}_{\text{self}}^{(l)} = \text{LayerNorm}(\mathbf{I}^{(l)} + \mathbf{O}_{\text{self}}^{(l)}). \quad (25)$$

Subsequently, the cross-attention output $\mathbf{O}_{\text{cross}}^{(l)}$ is integrated using the same residual architecture:

$$\mathbf{N}_{\text{cross}}^{(l)} = \text{LayerNorm}(\mathbf{N}_{\text{self}}^{(l)} + \mathbf{O}_{\text{cross}}^{(l)}). \quad (26)$$

The normalized output is then processed by a position-wise feed-forward network:

$$\mathbf{F}^{(l)} = \text{FFN}(\mathbf{N}_{\text{cross}}^{(l)}), \quad (27)$$

where the $\text{FFN}(\cdot)$ comprises two linear transformations with ReLU activation.

The final output of the l -th layer is obtained through the last residual connection and normalization, and then serves as the input to the subsequent Transformer layer ($l+1$):

$$\mathbf{I}^{(l+1)} = \text{LayerNorm}(\mathbf{N}_{\text{cross}}^{(l)} + \mathbf{F}^{(l)}). \quad (28)$$

2) *AEAT-AE Encoder: Environment-Aware Representation Learning*: The goal of the Transformer encoder is to produce a latent representation that captures both the signal structure and the impact of environmental parameters. For each Transformer layer $l \in \{1, \dots, L\}$, the signal representation is updated as:

$$\mathbf{I}^{(l)} = \text{TransformerLayer}(\mathbf{I}^{(l-1)}, \mathbf{E}_{\text{in}}), \quad \mathbf{I}^{(0)} = \mathbf{X}. \quad (29)$$

where $\mathbf{I}^{(l)} \in \mathbb{R}^{T \times d_k}$ contains encoded features at layer l . The final output $\mathbf{I}^{(L)}$ integrates signal dependencies conditioned on \mathbf{E}_{in} .

3) *AEAT-AE Decoder: Signal Recovery under Environmental Conditions*: The decoder aims to reconstruct the original signal using the received distorted signal \mathbf{Y} and the same environmental parameters \mathbf{E}_{in} . Each layer processes:

$$\mathbf{R}^{(l)} = \text{TransformerLayer}(\mathbf{R}^{(l-1)}, \mathbf{E}_{\text{in}}), \quad \mathbf{R}^{(0)} = \mathbf{Y}. \quad (30)$$

Here, $\mathbf{R}^{(l)} \in \mathbb{R}^{T \times d_k}$ denotes the output representation of the decoder at layer l . Each decoder layer applies self-attention to capture dependencies within the decoder input \mathbf{Y} , and cross-attention to integrate environmental context from \mathbf{E}_{in} . After L decoding layers, the final output is projected back to the signal domain via a linear layer:

$$\hat{\mathbf{X}} = \text{Linear}(\mathbf{R}^{(L)}), \quad (31)$$

where the linear layer restores the original signal dimensionality.

D. DQN-Based Adaptive Layer Selection in AEAT-AE

To address the computational complexity of Transformer structures and enhance adaptability to dynamic UAV-FSO channel conditions, AEAT-AE incorporates a DQN-based adaptive layer selection mechanism. Traditional approaches often rely on fixed-threshold strategies, which define specific environmental boundaries (e.g., for C_n^2 or AoA) to select decoding layers. While simple to implement, such static strategies are inherently rigid and depend on hand-crafted rules, making them difficult to generalize across complex and varying environments. In contrast, DQN formulates the layer selection problem as a Markov Decision Process (MDP), enabling dynamic and data-driven decision-making. By learning the action-value function $Q(s, a; \theta)$ via a neural network, DQN can efficiently handle high-dimensional, continuous state spaces and support real-time, scalable adaptation of decoding layers under fluctuating channel conditions.

Below, we detail the design of each component in this framework.

E. DQN-Based Adaptive Layer Selection in AEAT-AE

To address the computational complexity of Transformer structures and adapt to dynamic UAV-FSO channel conditions, adaptive layer selection methods mainly fall into threshold-based and RL-based approaches. Threshold-based methods rely on fixed environmental thresholds (e.g., C_n^2 , AoA), but designing effective thresholds that consider multiple simultaneous factors is impractical and inefficient, as handcrafted

rules cannot cover the vast, dynamic state space, leading to poor scalability and adaptability. Meanwhile, traditional tabular Q-learning faces the curse of dimensionality: discretizing multiple continuous variables exponentially expands the state-action space, causing large Q-tables that are costly to store and slow to train, thus unsuitable for complex UAV-FSO scenarios.

In contrast, DQN use neural networks to approximate the action-value function, naturally handling high-dimensional and continuous states. This allows efficient learning and generalization across diverse channel conditions without manual threshold design or discretization, enabling real-time, scalable adaptive layer selection.

1) *DQN Framework Tailored for AEAT-AE*: Below, we detail the key components of the DQN framework tailored for AEAT-AE.

State (s): The state s encodes the current environment as a continuous vector $\mathbf{E} = [Z, V_d, C_n^2, \sigma_s, \sigma_a]$, capturing diverse atmospheric and alignment factors. Prior to input into the DQN, this vector is normalized to ensure numerical stability and balanced feature scaling. Avoiding discretization preserves fine-grained variations, allowing the DQN to learn smooth, adaptive layer selection policies under dynamic channel conditions.

Action space (\mathcal{A}) consists of all possible subsets of Transformer layers to activate during inference. For a Transformer with L layers, each action $a \in \mathcal{A}$ specifies which layers are enabled; layers not selected operate as identity mappings, passing inputs through unchanged. This design effectively implements a dynamic masking of layers rather than altering the network architecture itself, allowing flexible adjustment of computational load without modifying the model structure.

$$L_a = |a|. \quad (32)$$

Reward (r): The immediate reward balances communication quality and computational cost, defined as

$$r = -(\lambda_{r_1} \cdot \text{BER} + \lambda_{r_2} \cdot L_a), \quad (33)$$

where $\lambda_{r_1}, \lambda_{r_2}$ regulate the trade-off between bit error rate (BER) and the number of activated layers L_a . This reward guides the agent towards minimizing decoding errors while reducing inference complexity.

Q-value Approximation and Learning: The agent employs a neural network parameterized by weights θ to approximate the action-value function $Q(s, a; \theta)$. The network is trained by minimizing the temporal difference loss

$$\mathcal{L}(\theta) = \mathbb{E}_{(s,a,r,s')} \left[\left(r + \gamma \max_{a'} Q(s', a'; \theta^-) - Q(s, a; \theta) \right)^2 \right], \quad (34)$$

where the tuple (s, a, r, s') consists of the current state s , action a , received reward r , and the subsequent state s' . The variable a' denotes possible next actions in the next state s' . Here, θ^- refers to the parameters of a periodically updated target network that stabilizes training, and γ is the discount factor reflecting the importance of future rewards.

Experience Replay: Transitions (s, a, r, s') are stored in a prioritized replay buffer \mathcal{D} . Sampling based on temporal difference errors focuses training on more informative experiences, enhancing sample efficiency and convergence speed.

Policy Update and Inference: The DQN agent updates θ iteratively via gradient descent on $\mathcal{L}(\theta)$. During inference, given the current state s , the optimal action a^* is selected as

$$a^* = \arg \max_a Q(s, a; \theta). \quad (35)$$

By adaptively selecting the most informative Transformer layers based on environmental conditions, the system reduces computation and overfitting while ensuring robust reconstruction. The DQN's function approximation efficiently handles high-dimensional states, enabling real-time, data-driven optimization beyond heuristic or fixed rules.

2) *DQN-Based Training and Deployment Process:* The DQN-based resource allocation strategy operates in two stages: **training** and **deployment**, enabling the system to autonomously adapt to dynamic environments through deep function approximation.

During the **training phase**, a neural network is used to approximate the Q-value function $Q(s, a; \theta)$. At each time step, given a current **state** s , the controller selects an **action** a using an ε -greedy policy:

$$a = \begin{cases} \text{random action,} & \text{with probability } \varepsilon, \\ \arg \max_{a'} Q(s, a'; \theta), & \text{with probability } 1 - \varepsilon, \end{cases} \quad (36)$$

After applying the selected Transformer layers, the system evaluates performance, receives a reward r , observes the new state s' , and stores the transition (s, a, r, s') in a replay buffer. The DQN is then trained by minimizing the temporal difference loss as shown in (34). During the **deployment phase**, the system directly uses the trained DQN to select the optimal action (a^*) for a given state.

To ensure system stability and avoid unnecessary reconfigurations, the controller updates the Transformer configuration **only when significant changes in environmental parameters are detected**. This strategy balances adaptability and computational efficiency while maintaining robust communication performance.

F. Overall AEAT-AE Structure

To unify training of the Transformer-AE and the DQN-based layer selection, we propose the AEAT-AE framework, which jointly optimizes signal reconstruction quality and layer efficiency. This enables dynamic adaptation to changing environments while maintaining both computational efficiency and communication performance. The overall algorithm is summarized in Algorithm 1.

While the DQN reward function is defined in (34), directly using bit error rate (BER) poses a challenge due to its non-differentiability. As a practical solution, we adopt the mean squared error (MSE) between the transmitted and reconstructed signals as a surrogate reward:

$$\mathcal{L}_{\text{MSE}} = \|\mathbf{X} - \hat{\mathbf{X}}\|^2, \quad (37)$$

Algorithm 1 Training and Deployment of AEAT-AE with DQN-Based Adaptive Layer Selection

Require: Input binary signal \mathbf{s} ; environment parameters $\mathbf{E} = [Z, V_d, C_n^2, \sigma_s, \sigma_a]$; channel coefficient \mathbf{H} ; AWGN noise \mathbf{w}

Ensure: Reconstructed signal $\hat{\mathbf{s}}$

- 1: **Step 1: Full-depth Training of AEAT-AE**
- 2: Define subroutine: $\hat{\mathbf{s}} = \text{AEAT_AE}(\mathbf{s}, \mathbf{H}, \mathbf{w}, a)$
- 3: Action $a \subseteq \{0, 1, \dots, L-1\}$ denotes the subset of Transformer layers selected for activation
- 4: Embed input: $\mathbf{X} = \text{Embed}(\mathbf{s})$
- 5: Encode: $\mathbf{x} = \text{Encoder}(\mathbf{X}; \theta_{\text{enc}}, a)$
- 6: Channel transmission: $\mathbf{y} = \mathbf{H} \cdot \mathbf{x} + \mathbf{w}$
- 7: Decode: $\hat{\mathbf{s}} = \text{Decoder}(\mathbf{y}; \theta_{\text{dec}}, a)$
- 8: **Return** $\hat{\mathbf{s}}$
- 9: Compute binary cross-entropy loss:

$$\mathcal{L}_{\text{AE}} = \sum_{n=1}^N [s_n \log(\hat{s}_n) + (1 - s_n) \log(1 - \hat{s}_n)]$$

- 10: Update parameters $\theta_{\text{AE}} = \theta_{\text{enc}} \cup \theta_{\text{dec}}$ via gradient descent:

$$\mathcal{L}_{\text{total}} = \lambda_1 \mathcal{L}_{\text{AE}} + \lambda_4 \|\theta_{\text{AE}}\|^2$$

- 11: **Step 2: DQN-Based Adaptive Layer Selection**
- 12: Freeze θ_{AE} ; initialize DQN network $Q(s, a; \theta)$ and target network $Q(s, a; \theta^-)$
- 13: Initialize replay buffer \mathcal{D}
- 14: **for** each training episode **do**
- 15: Sample environment parameters \mathbf{E} and normalize as state s
- 16: Select action a_t using ε -greedy policy over $Q(s, a; \theta)$
- 17: Reconstruct signal: $\hat{\mathbf{s}} = \text{AEAT_AE}(\mathbf{s}, \mathbf{H}, \mathbf{w}, a_t)$
- 18: Compute MSE loss: $\mathcal{L}_{\text{MSE}} = \|\hat{\mathbf{s}} - \mathbf{s}\|^2$
- 19: Count activated layers: $L_{a_t} = |a_t|$
- 20: Compute reward:

$$r_t = -(\lambda_2 \cdot \mathcal{L}_{\text{MSE}} + \lambda_3 \cdot L_{a_t})$$

- 21: Observe next state s'
- 22: Store transition (s, a_t, r_t, s') in buffer \mathcal{D}
- 23: Sample mini-batch (s_i, a_i, r_i, s'_i) from \mathcal{D}
- 24: Compute TD target:

$$y_i = r_i + \gamma \max_{a'} Q(s'_i, a'; \theta^-)$$

- 25: Update DQN by minimizing loss:

$$\mathcal{L}_{\text{DQN}} = \frac{1}{B} \sum_i (y_i - Q(s_i, a_i; \theta))^2$$

- 26: Periodically update target network: $\theta^- \leftarrow \theta$
- 27: **end for**
- 28: **Step 3: AEAT-AE Deployment**
- 29: Observe current environment parameters \mathbf{E} and normalize as state s
- 30: Select optimal action: $a^* = \arg \max_a Q(s, a; \theta)$
- 31: Reconstruct signal: $\hat{\mathbf{s}} = \text{AEAT_AE}(\mathbf{s}, \mathbf{H}, \mathbf{w}, a^*)$
- 32: If significant change in \mathbf{E} is detected, remap to s' and reselect action a^*

where \mathbf{X} and $\hat{\mathbf{X}}$ denote the transmitted and reconstructed signals, respectively. The use of MSE as a continuous approximation of BER enables stable and efficient training via gradient-based optimization.

Although BER is the standard metric for evaluating communication reliability, it is non-differentiable and unsuitable for guiding gradient-based learning in the DQN module. To address this, we adopt MSE as a surrogate reward signal for the Q-network. While MSE does not directly capture discrete

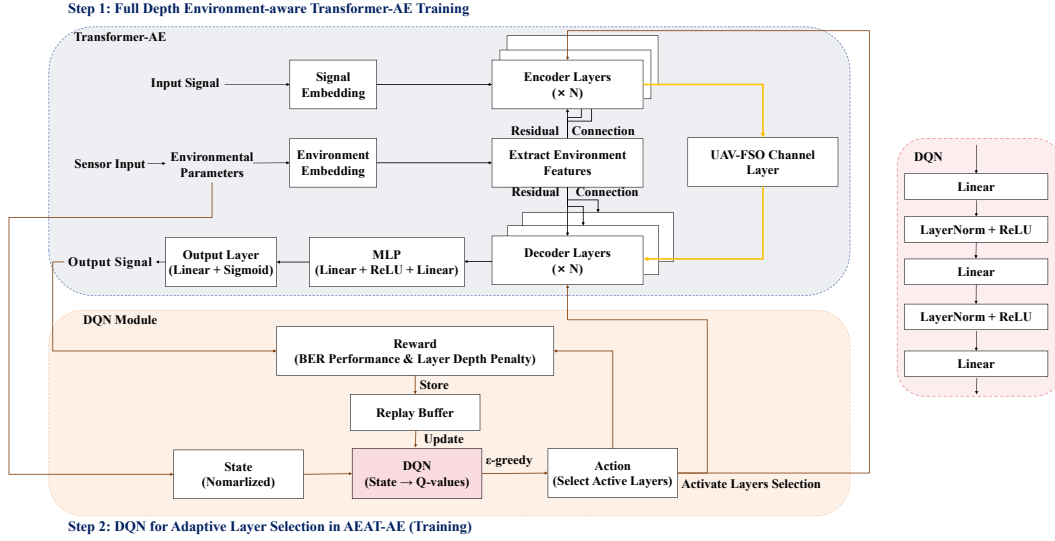


Fig. 5. Training process of AEAT-AE.

symbol errors, it remains well correlated with BER in high-SNR regimes and penalizes all deviations in the signal space, making it a finer-grained and more sensitive training signal. This promotes stable convergence and improved reconstruction fidelity. Importantly, while MSE is used during training for reward approximation, final evaluations and comparisons are still based on BER, ensuring fair benchmarking aligned with communication objectives.

The Transformer-AE itself is trained using the standard cross-entropy loss:

$$\mathcal{L}_{\text{AE}}(\mathbf{X}, \hat{\mathbf{X}}) = - \sum_{n=1}^N \left(X_n \log(\hat{X}_n) + (1 - X_n) \log(1 - \hat{X}_n) \right). \quad (38)$$

We define the **overall learning objective** of AEAT-AE, separating the optimization targets for the Transformer-AE and the DQN-based policy network:

$$\min_{\theta_{\text{AE}}, \theta_Q} \mathbb{E}_{\mathbf{E}, a_t, \mathbf{X}} \left[\lambda_1 \mathcal{L}_{\text{AE}}(\mathbf{X}, \hat{\mathbf{X}}) + \lambda_2 (Q(s_t, a_t; \theta_Q) - y_t)^2 + \lambda_3 \|\theta_Q\|^2 + \lambda_4 \|\theta_{\text{AE}}\|^2 \right]. \quad (39)$$

where θ_{AE} and θ_Q denote parameters of the Transformer-AE and Q-network, respectively. The TD target is $y_t = r_t + \gamma \max_{a'} Q(s_{t+1}, a'; \theta_Q^-)$, with θ_Q^- as the target network parameters. The coefficients λ_1 through λ_4 balance reconstruction, policy learning, and regularization terms.

This joint optimization is constrained by:

$$\text{s.t.} \begin{cases} L_{\min} \leq L_a \leq L, \\ a_t \in \mathcal{A}, \\ a_t = \arg \max_a Q(s_t, a; \theta), \end{cases} \quad (40)$$

where t denotes the time step, $a_t \in \mathcal{A}$ is the action selected by the DQN (i.e., a subset of Transformer layers), and $Q(s_t, a; \theta)$ is the action-value function parameterized by neural network weights θ . The constraint $L_{\min} \leq L_a \leq L$ ensures that a minimal model capacity is preserved.

1) *Training Process*: As shown in Fig. 5, the training process consists of two key stages:

- **Full-depth Transformer-AE Training**: The Transformer-AE is first trained with all layers active to ensure generalization across diverse environments.
- **DQN-based Layer Selection**: A DQN agent is trained to learn the mapping from environmental states to optimal Transformer layer configurations. The pretrained Transformer-AE is used to evaluate the reward for each state-action pair, considering both reconstruction performance and computational cost.

Through iterative DQN updates, the system gradually learns an adaptive policy that selects the most efficient layer subsets during deployment, enabling dynamic complexity control based on the current environment.

2) *Deployment Process*: During deployment, the model architecture remains identical to that used in training, except that no parameter updates are performed. The DQN agent leverages real-time environmental states to select appropriate Transformer layers, dynamically activating only the necessary ones. Inactive layers are replaced with identity mappings, ensuring signal propagation while reducing computational cost.

Importantly, the DQN agent no longer updates its policy or receives reward feedback during deployment. Instead, it uses the trained Q-network to infer optimal layer selection decisions based on current environmental inputs. The policy remains fixed under stable conditions, while significant environmental changes trigger new inferences from the Q-network, allowing the model to adapt quickly with minimal overhead.

IV. SIMULATION RESULTS

A. Experiment Setup

During training, the UAV-FSO channel is simulated in MATLAB to generate fading coefficients, which are embedded into the channel layer of the model. The key environmental and channel parameters used in this simulation are listed

TABLE II
CHANNEL SIMULATION VARIABLES SETTINGS

| Variable | Value | Variable | Value |
|-----------------------|----------------------------------|-------------------|--------------------------------|
| σ_s | $0.01 \leq \sigma_s \leq 0.05$ m | ρ | 0.596 |
| η_e | 0.5 | $\phi_A - \phi_B$ | $\pi/2$ |
| σ_a | $2 \leq \sigma_a \leq 5$ mrad | Ω | 1.3265 |
| σ_w^2 | 10^{-10} | η_e | 0.5 |
| b_0 | 0.1079 | λ | 1550 nm |
| α | 8.2 | β | 4 |
| r_a | 0.1 m | w_{oz} | 2 m |
| θ_{FoV} | 20 mrad | V_d | $2 \leq V_d \leq 13$ km |
| Z | $1 \leq Z \leq 5$ km | C_n^2 | {5e-14, 1.7e-14, 5e-15, 4e-15} |

in Table II. To enhance generalization, each environmental parameter $\mathbf{E} = [Z, V_d, C_n^2, \sigma_s, \sigma_a]$ is randomly sampled within its specified range, thereby exposing the model to diverse channel conditions. The SNR is fixed at 10 dB to ensure stable training and allow the model to focus on learning from environmental variations without noise interference.

For evaluation, the model is tested across a range of SNRs to assess robustness under different channel conditions. An independent test set is generated using the same parameter ranges as training, but with no overlap, avoiding data leakage. BER performance is measured via large-scale Monte Carlo simulations.

The DQN-based controller takes normalized continuous environmental parameters as input, enabling efficient and generalizable layer selection. Table III summarizes the key hyperparameters used in the AEAT-AE framework, covering both the Transformer-AE and the DQN-based adaptive layer selection.

TABLE III
PARAMETER SETTINGS FOR AEAT-AE

| Transformer-AE Settings | |
|-----------------------------------|--------------------|
| Sequence length T | 16 |
| Embedding dimension | 32 |
| Number of attention heads N_h | 4 |
| Number of Transformer layers L | 4 |
| Initial active layers | [0, 1, 2, 3] |
| Environmental parameter dimension | 5 |
| Batch size | 64 |
| Transformer-AE training epochs | 50 |
| Learning rate | 0.001 |
| Fixed training SNR | 10 dB |
| DQN Settings | |
| State dimension | 5 |
| Learning rate | 3×10^{-4} |
| Discount factor γ | 0.99 |
| Soft target update rate τ | 1×10^{-3} |
| Initial ϵ | 1.0 |
| Minimum ϵ | 0.01 |
| ϵ decay rate | 0.995 |
| Replay memory size | 100000 |
| Batch size | 128 |
| Prioritized replay alpha | 0.6 |
| Prioritized replay beta | 0.4 |
| Optimizer | AdamW |
| Learning rate scheduler | CosineAnnealingLR |

B. Performance Results

To better analyze each component's contribution, we define several variants of our Transformer-AE (T-AE). **T-AE (no env, no Q)** disables both environmental guidance and DQN-based layer selection; **T-AE (env, no Q)** includes environmental inputs but uses a fixed Transformer depth; **T-AE (no env, Q)** applies adaptive layer selection via DQN without environmental inputs; and **T-AE with env & Q**, which incorporates both, corresponds to our **AEAT-AE** design. These variants help isolate the effects of environmental adaptation and dynamic computation.

1) *Impact of Environmental Awareness on System Robustness*: To highlight the impact of environmental parameters in our proposed AEAT-AE framework, we conduct ablation experiments by removing environmental inputs and comparing the resulting BER performance.

Fig. 6 presents performance comparisons in two subfigures. Fig. 6 (a) shows BER versus SNR for various schemes, including our proposed methods, baselines (OOK, 16QAM), traditional autoencoders (FCN-AE [20], CNN-AE [25], [26]), and classic coding schemes: Hamming (7,4) and LDPC (200,5,10) with code rate 0.5. Theoretical BER curves for OOK and Hamming (7,4) under AWGN channels are included for reference. Fig. 6 (b) plots the inference time against BER to process a 200,000-bit stream, using consistent markers and colors from (a). The x-axis is logarithmic to cover the wide range of inference times.

Among the baselines, OOK and 16QAM exhibit the shortest inference times due to the absence of encoding or decoding modules, but their BER performance degrades significantly under UAV-FSO channel conditions, as they are not robust to channel distortions. For traditional coded schemes, Hamming (7,4) shows a notable performance gap between hard and soft decoding. LDPC provides strong error correction and low BER but requires longer code lengths to fully realize its advantages, resulting in high decoding complexity that limits its practicality in many scenarios. In comparison, both FCN and CNN outperform uncoded baselines, especially at low SNRs. CNN achieves better BER than FCN due to stronger feature extraction, though with moderately increased inference time.

Our proposed Transformer-AE variants achieve a favorable trade-off between communication performance and computational efficiency. Without incorporating environmental inputs, the baseline Transformer-AE yields BER performance that falls between those of FCN- and CNN-based AEs. When environmental features are introduced via cross-attention and residual fusion, and the model is trained under the same number of epochs, the BER is further reduced by an average of **83.53%** compared to the baseline Transformer-AE, as shown in the purple shaded region of Fig. 6 (a). This highlights the effectiveness of environmental integration, which is further validated through ablation studies showing significant performance degradation when these inputs are removed.

Importantly, this improvement in BER does not come at the expense of inference efficiency. Although the overall complexity is higher than uncoded schemes (as expected due to added encoding and decoding stages), the inference time

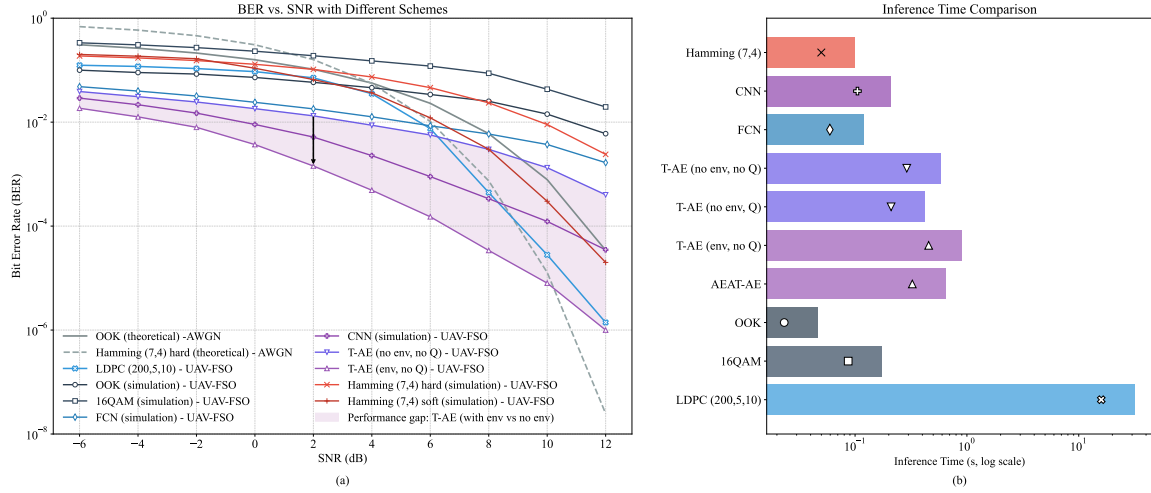


Fig. 6. Comparison of different schemes: (a) BER vs. SNR, including effects of environmental input; (b) Inference time of these methods for a 200,000-bit stream.

of the Transformer-based model remains comparable to that of CNN and FCN baselines. This demonstrates that AEAT-AE can effectively balance robustness and runtime, making it suitable for real-time UAV-FSO communication scenarios.

Fig. 6 (b) further compares the full Transformer-AE with its adaptive variant. By integrating a DQN-based policy network to dynamically activate a subset of Transformer layers, the adaptive model (AEAT-AE) achieves reduced inference latency under varying conditions while maintaining competitive BER. Although AEAT-AE introduces neural processing overhead compared to OOK/16QAM, it offers considerable improvements in BER and maintains inference latency comparable to FCN/CNN-based autoencoders. Therefore, our claim of efficiency refers not to absolute speed but to the favorable trade-off between accuracy and computational complexity. In particular, AEAT-AE achieves BER performance close to or better than LDPC in our test conditions, while incurring significantly lower decoding latency, making it promising for latency-sensitive, high-throughput scenarios.

2) DQN-Based Adaptive Layer Selection for Efficient Inference: In our proposed AEAT-AE, the Transformer-AE demonstrates strong feature extraction capabilities and fast convergence. As shown in Fig. 7, with the same fixed layer configuration, it achieves BER performance comparable to or better to that of FCN- and CNN-based autoencoders (evaluated over 50 to 200 epochs), despite being trained for only 50 epochs. This underscores the efficiency of the model in both training and inference.

To further improve inference efficiency, AEAT-AE integrates a DQN-based adaptive layer selection mechanism that dynamically decides which Transformer layers to activate based on environmental inputs. Instead of explicitly controlling network depth, the DQN agent selects a subset of layers to execute, with inactive layers replaced by identity mappings that simply forward inputs unchanged. This selective activation effectively modulates computational complexity, which can be quantitatively measured by the average number of activated layers.

Fig. 8 presents ablation results comparing the full-depth Transformer-AE (4 encoder + 4 decoder layers, total 8 layers) with its DQN-enabled variant under varying SNRs. We report BER (left axis) alongside the average number of active layers (right axis), both with and without environmental input. On average, the DQN agent reduces activated layers by **4.39** without environmental information and **5.13** when environmental features are included, demonstrating significant computational savings.

Importantly, the experimental results show that more layers are activated at low SNR to maintain accuracy, while fewer layers are used at high SNR to reduce computation without BER loss - behavior that aligns well with intuitive expectations. Around 6 dB SNR, the DQN-controlled model achieves both improved BER and lower layer usage compared to the fixed full-depth baseline. Incorporating environment-aware inputs further reduces the number of active layers without degrading performance, highlighting the benefit of environment-guided inference. These findings confirm that the DQN-based layer selection effectively balances robustness and efficiency in dynamic UAV-FSO channels.

3) Image Transmission Performance Under Severe Channel Conditions: To intuitively demonstrate the practical effectiveness of the proposed method, we present a visual case study of image transmission and reconstruction over a UAV-FSO channel under adverse conditions. For fair comparison, all input images are standardized to three-channel RGB with a white background, quantized to 8 bits per channel, converted into a binary bitstream, zero-padded to match the fixed input length, and segmented into equal-length sequences for modulation and transmission through the transmitter-side autoencoder over the simulated UAV-FSO channel.

At the receiver, the decoder output is thresholded at 0.5 to regenerate the binary bitstream, which is then truncated to the original length prior to padding. The bitstream is decoded back into 8-bit pixel values and reshaped to reconstruct the original image dimensions. Reconstruction quality is evaluated by the Peak Signal-to-Noise Ratio (PSNR), defined as:

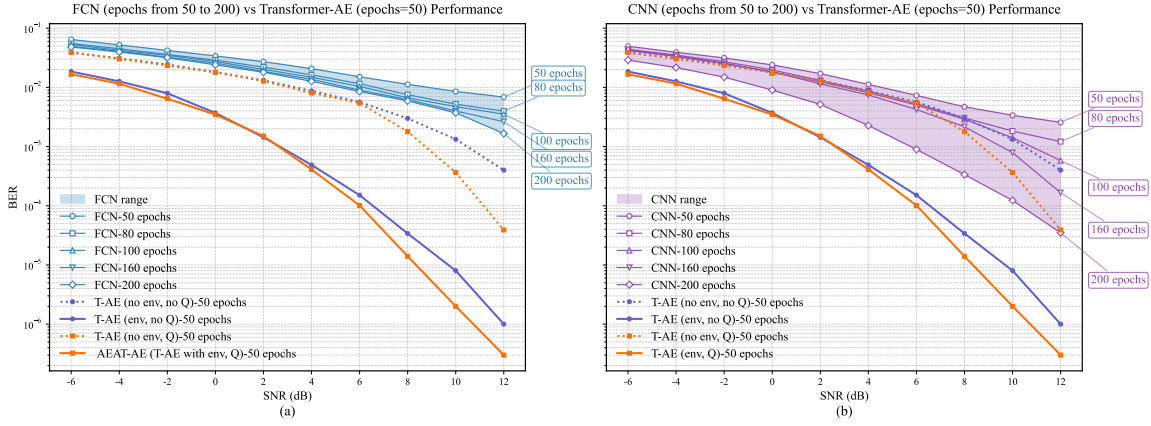


Fig. 7. BER vs. SNR at different training epochs for (a) FCN and Transformer-AE, (b) CNN and Transformer-AE.

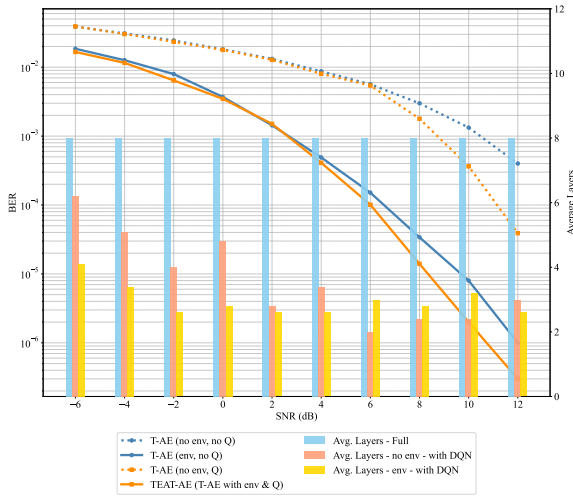


Fig. 8. BER Performance and Average Layers vs. SNR

$$\text{PSNR} = 10 \cdot \log_{10} \left(\frac{\text{MAX}^2}{\text{MSE}} \right), \quad (41)$$

where $\text{MAX} = 255$ is the maximum pixel value, and MSE is the mean squared error between the original and reconstructed images. Higher PSNR indicates better visual fidelity.

Under extremely low SNR conditions, the FCN-based scheme results in reconstructions with substantial noise, while the CNN-based model offers modest improvements but still exhibits noticeable degradation, particularly at SNR values of -16 dB and -20 dB. In comparison, the environment-aware Transformer-based approaches, namely **T-AE (env, no Q)** and the proposed **AEAT-AE**, produce relatively clearer images and higher PSNR, indicating enhanced robustness against channel impairments. Both methods effectively utilize environmental information, whereas **AEAT-AE** further incorporates adaptive layer selection through DQN. This allows it to achieve comparable or improved reconstruction quality relative to **T-AE (env, no Q)**, while also reducing computational cost. These results suggest that **AEAT-AE** offers a balanced trade-off between efficiency and performance under challenging SNR conditions.

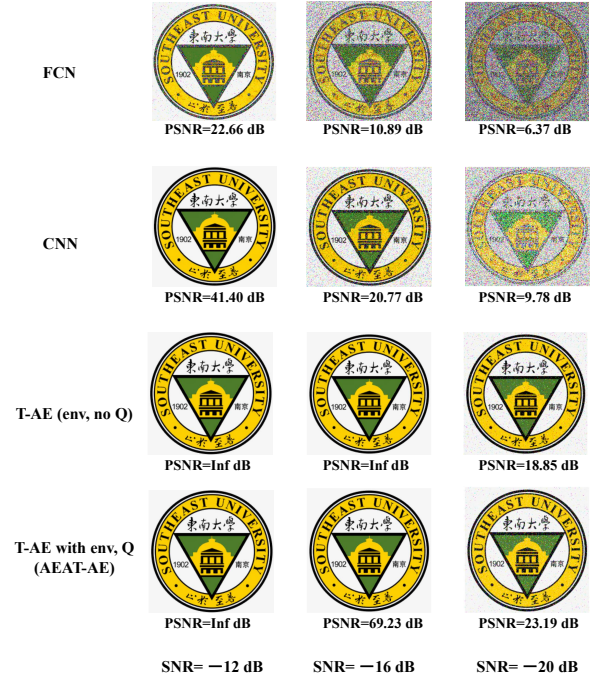


Fig. 9. Image Transmission Performance under Different Schemes

V. DISCUSSION

This study uses comprehensive, controlled simulations as a necessary first step in UAV-FSO research, serving as a pilot investigation that demonstrates the feasibility and effectiveness of the **AEAT-AE** framework with DQN-based adaptive layer selection. Our focus is on validating design and adaptability under diverse channel conditions, laying groundwork for future real-world deployment and refinement.

Given practical systems' stringent real-time and complexity constraints, further work on more lightweight adaptive strategies is warranted. While deep reinforcement learning offers enhanced adaptability, the current DQN strikes a practical balance between performance and computational cost suitable for edge deployment. Future research may consider more advanced DRL methods if they offer clear gains in adaptability or control precision.

VI. CONCLUSION

In this work, we introduced the Adaptive Environment-aware Transformer-AE (AEAT-AE) framework for UAV-FSO communication, which leverages environmental parameters and reinforcement learning to enhance both robustness and efficiency. By incorporating environmental awareness through cross-attention and introducing a DQN-driven adaptive layer selection mechanism, AEAT-AE effectively adapts to varying channel conditions while minimizing computational complexity. Extensive simulations demonstrate significant improvements in key performance metrics, including BER, PSNR, and layer efficiency, especially in challenging SNR scenarios. The results validate the practical feasibility of AEAT-AE for UAV-FSO deployments, positioning it as a promising solution for next-generation, adaptive optical wireless communication systems that can operate efficiently under dynamic and fluctuating conditions.

REFERENCES

- [1] C.-X. Wang et al., "On the Road to 6G: Visions, Requirements, Key Technologies, and Testbeds," *IEEE Commun. Surv. Tutorials*, vol. 25, no. 2, pp. 905–974, 2023.
- [2] A. K. Majumdar and J. C. Ricklin, Eds., *Free-space laser communications: principles and advances. in Optical and fiber communications reports*, no. 2. New York, NY: Springer, 2008.
- [3] M. Z. Chowdhury, Md. Shahjalal, S. Ahmed, and Y. M. Jang, "6G Wireless Communication Systems: Applications, Requirements, Technologies, Challenges, and Research Directions," *IEEE Open J. Commun. Soc.*, vol. 1, pp. 957–975, 2020.
- [4] Z. Zhang et al., "Optical Mobile Communications: Principles, Implementation, and Performance Analysis," *IEEE Trans. Veh. Technol.*, vol. 68, no. 1, pp. 471–482, Jan. 2019.
- [5] W. Fawaz, C. Abou-Rjeily, and C. Assi, "UAV-Aided Cooperation for FSO Communication Systems," *IEEE Commun. Mag.*, vol. 56, no. 1, pp. 70–75, Jan. 2018.
- [6] M. T. Dabiri, S. M. S. Sadough, and M. A. Khalighi, "Channel Modeling and Parameter Optimization for Hovering UAV-Based Free-Space Optical Links," *IEEE J. Select. Areas Commun.*, vol. 36, no. 9, pp. 2104–2113, Sep. 2018.
- [7] H.-B. Jeon et al., "Free-Space Optical Communications for 6G Wireless Networks: Challenges, Opportunities, and Prototype Validation," *IEEE Commun. Mag.*, vol. 61, no. 4, pp. 116–121, Apr. 2023.
- [8] M. Mahmood, M. Ghadaksaz, A. Koc, and T. Le-Ngoc, "Deep Learning Meets Swarm Intelligence for UAV-Assisted IoT Coverage in Massive MIMO," *IEEE Internet Things J.*, vol. 11, no. 5, pp. 7679–7696, Mar. 2024.
- [9] D. Menaka, S. Gauni, C. T. Manimegalai, and K. Kalimuthu, "Vision of IoT: advances and future trends in optical wireless communication," *J Opt*, vol. 50, no. 3, pp. 439–452, Sep. 2021.
- [10] L. J. S. Kumar, P. Krishnan, B. Shreya, and S. M.S., "Performance enhancement of FSO communication system using machine learning for 5G/6G and IoT applications," *Optik*, vol. 252, p. 168430, Feb. 2022.
- [11] Y. C. Manie, C.-K. Yao, T.-Y. Yeh, Y.-C. Teng, and P.-C. Peng, "Laser-Based Optical Wireless Communications for Internet of Things (IoT) Application," *IEEE Internet Things J.*, vol. 9, no. 23, pp. 24466–24476, Dec. 2022.
- [12] M. Z. Chowdhury, Md. Shahjalal, Moh. K. Hasan, and Y. M. Jang, "The Role of Optical Wireless Communication Technologies in 5G/6G and IoT Solutions: Prospects, Directions, and Challenges," *Applied Sciences*, vol. 9, no. 20, p. 4367, Oct. 2019.
- [13] M. R. Hayal et al., "Modeling and investigation on the performance enhancement of hovering UAV-based FSO relay optical wireless communication systems under pointing errors and atmospheric turbulence effects," *Opt Quant Electron*, vol. 55, no. 7, p. 625, Jul. 2023.
- [14] F. Nadeem, V. Kvicera, M. Awan, E. Leitgeb, S. Muhammad, and G. Kandas, "Weather effects on hybrid FSO/RF communication link," *IEEE J. Select. Areas Commun.*, vol. 27, no. 9, pp. 1687–1697, Dec. 2009.
- [15] M. P. Bart et al., "Deep learning for enhanced free-space optical communications," *Mach. Learn.: Sci. Technol.*, vol. 4, no. 4, p. 045046, Dec. 2023.
- [16] H. Zeng, H. Wang, K. Wang, X. Yu, and Z. Zhang, "Enhancing Robustness in Hybrid FSO/RF Systems: A Feedback-Free Approach Leveraging Deep Learning for Real-Time Power Allocation," *IEEE Internet Things J.*, pp. 1–1, 2025.
- [17] C. Zheng, S. Yu, and W. Gu, "A SVM-based processor for free-space optical communication," in 2015 IEEE 5th International Conference on Electronics Information and Emergency Communication, Beijing, China: IEEE, May 2015, pp. 30–33.
- [18] W. Chen et al., "Deep Learning-Based Channel Modeling for Free Space Optical Communications," *J. Lightwave Technol.*, vol. 41, no. 1, pp. 183–198, Jan. 2023.
- [19] H. Lu, M. Jiang, and J. Cheng, "Deep Learning Aided Robust Joint Channel Classification, Channel Estimation, and Signal Detection for Underwater Optical Communication," *IEEE Trans. Commun.*, vol. 69, no. 4, pp. 2290–2303, Apr. 2021.
- [20] T. O'Shea and J. Hoydis, "An Introduction to Deep Learning for the Physical Layer," *IEEE Trans. Cogn. Commun. Netw.*, vol. 3, no. 4, pp. 563–575, Dec. 2017.
- [21] V. Raj and S. Kalyani, "Backpropagating Through the Air: Deep Learning at Physical Layer Without Channel Models," *IEEE Commun. Lett.*, vol. 22, no. 11, Nov. 2018, pp. 2278–81.
- [22] M. Soltani, W. Fatnassi, A. Aboutaleb, Z. Rezki, A. Bhuyan, and P. Titus, "Autoencoder-Based Optical Wireless Communications Systems," in 2018 IEEE Globecom Workshops (GC Wkshps), Abu Dhabi, United Arab Emirates: IEEE, Dec. 2018, pp. 1–6.
- [23] F. A. Aoudia and J. Hoydis, "Model-Free Training of End-to-End Communication Systems," *IEEE JSAC*, vol. 37, no. 11, Nov. 2019, pp. 2503–16.
- [24] Z.-R. Zhu, J. Zhang, R.-H. Chen, and H.-Y. Yu, "Autoencoder-Based Transceiver Design for OWC Systems in Log-Normal Fading Channel," *IEEE Photonics J.*, vol. 11, no. 5, pp. 1–12, Oct. 2019.
- [25] H. Ye, L. Liang, G. Y. Li, and B.-H. Juang, "Deep Learning-Based End-to-End Wireless Communication Systems With Conditional GANs as Unknown Channels," *IEEE Trans. Wireless Commun.*, vol. 19, no. 5, pp. 3133–3143, May 2020.
- [26] D. B. Kurka and D. Gündüz, "DeepJSCC-f: Deep Joint Source-Channel Coding of Images With Feedback," in *IEEE Journal on Selected Areas in Information Theory*, vol. 1, no. 1, pp. 178–193, May 2020.
- [27] X. Liu, Z. Wei, A. Pepe, Z. Wang, and H. Y. Fu, "Autoencoder for Optical Wireless Communication System in Atmospheric Turbulence," in 2020 Opto-Electronics and Communications Conference (OECC), Taipei, Taiwan: IEEE, Oct. 2020, pp. 1–3.
- [28] A. E.-R. A. El-Fikky and Z. Rezki, "On the Performance of Autoencoder-Based Space Optical Communications," in *GLOBECOM 2022 - 2022 IEEE Global Communications Conference*, Rio de Janeiro, Brazil: IEEE, Dec. 2022, pp. 1466–1471.
- [29] A. Elfikky, M. Soltani, and Z. Rezki, "Learning-Based Autoencoder for Multiple Access and Interference Channels in Space Optical Communications," *IEEE Commun. Lett.*, vol. 27, no. 10, pp. 2662–2666, Oct. 2023.
- [30] A. Elfikky, M. Soltani, and Z. Rezki, "End-to-End Learning Framework for Space Optical Communications in Non-Differentiable Poisson Channel," *IEEE Wireless Commun. Lett.*, vol. 13, no. 8, pp. 2090–2094, Aug. 2024.
- [31] H. Safi, I. Tavakkolnia, and H. Haas, "Deep Learning Based End-to-End Optical Wireless Communication Systems With Autoencoders," *IEEE Commun. Lett.*, vol. 28, no. 6, pp. 1342–1346, Jun. 2024.
- [32] Y. Li, "Deep Reinforcement Learning: An Overview," Nov. 26, 2018, arXiv: arXiv:1701.07274.
- [33] J. Fan, Z. Wang, Y. Xie, and Z. Yang, "A Theoretical Analysis of Deep Q-Learning," Feb. 24, 2020, arXiv: arXiv:1901.00137.
- [34] L. P. Kaelbling, M. L. Littman, A. W. Moore, and S. Hall, "Reinforcement Learning: A Survey," *Reinforcement Learning*.
- [35] I. S. Ansari, F. Yilmaz, and M.-S. Alouini, "Performance Analysis of Free-Space Optical Links Over Málaga (\mathcal{M}) Turbulence Channels With Pointing Errors," *IEEE Trans. Wireless Commun.*, vol. 15, no. 1, pp. 91–102, Jan. 2016.
- [36] G. Xu, S. Lu, L. Qu, Q. Zhang, Z. Song, and B. Ai, "Outage Probability and Average BER of UAV-Assisted RF/FSO System for Space–Air–Ground Integrated Networks Under Angle-of-Arrival Fluctuations," *IEEE Internet Things J.*, vol. 11, no. 20, pp. 34009–34023, Oct. 2024.
- [37] D. Singh and S. R., "Comprehensive Performance Analysis of Hovering UAV-Based FSO Communication System," *IEEE Photonics J.*, vol. 14, no. 5, pp. 1–13, Oct. 2022, doi: 10.1109/JPHOT.2022.3205704.